Supporting information

Electrochemical Surface Reconstructed $Pt_{x(x=2,3)}Si$/PtSi/p-Si Photocathodes for Achieving High Efficiency in Photoelectrochemical H_2 Generation

Haoyue Zhang,[a,c] *Guangwei She,*[a]* *Jing Xu,*[b] *Shengyang Li,*[a,c] *Yun Liu,*[d] *Jun Luo*[b]*,[c] *and Wensheng Shi*[a,c,e]

[a] Key Laboratory of Photochemical Conversion and Optoelectronic Materials, Technical Institute of Physics and Chemistry, Chinese Academy of Sciences, Beijing 100190, China

[b] Key Laboratory of Microelectronic Devices & Integrated Technology, Institute of Microelectronics, Chinese Academy of Sciences, Beijing 10009, China

[c] University of Chinese Academy of Sciences, Chinese Academy of Sciences, Beijing 100049, China

[d] Research School of Chemistry, The Australian National University, Canberra, ACT 2601, Australia

[e] Ganjiang Innovation Academy, Chinese Academy of Sciences, Ganzhou 341000, China

Supplementary Notes

Structural characterization measurements

TEM, HRTEM and HADDF-TEM were executed with a JEOL analytic transmission electron microscope with *in-situ* double spherical aberration correction (JEM-ARM300F).

GI-XRD was executed with a Brucker D8 Discover using Cu Kα radiation, operating at 40 kV and 40 mA. And the glancing angle was 0.5 °.

XPS spectra of Pt 4f were performed on Thermofisher Scientific ESCALAB 250Xi with an Al K-alpha X-ray source. The measurement parameters were as mentioned below: spot size of 650 μm; pass energy of 30 eV; energy step of 0.1 eV; dwell time of 34.6 s; 3 scans. The peak energies were calibrated with the C 1s peak binding energy, which was calibrate to be 284.8 eV.

SIMS was executed with an elemental and isotopic Microanalysis equipment CAMECA sims 4500.

Mott-Schottky measurements

In order to conduct the Mott-Schottky measurements, the photocathodes were capsulated to solid-state cells. First, the samples were cut into 1×0.5 cm^2 size slices. Then, the p-Si back was covered by InGa eutectic layer to create ohmic contact. And a Cu foil was contacted to the InGa eutectic layer as the counter and reference electrode after fixed by epoxy resin. Elargol was smeared evenly on the front of the sample to make favorable conductivity as the working electrode. The Mott-Schottky plots of the solid-state cells were measured in dark with the AC potential frequency of 100 kHz on the CHI660C workstation.[1]

Calculation of SBH and ABPE

The SBH (ϕ_b) was calculated by the following equation according to the

illustration of energy band structure shown in Fig. S1:

$$\phi_{bp} = E_{fb} + V_p$$

where E_{fb} is the flat band potential, which could be obtained from following equation:

$$E_{fb} = b + \frac{KT}{q}$$

where b is the x-axis intercept of the Mott-Schottky plots linear fitting line from Fig. 2a, which is 0.65 eV. K is Boltzmann constant 1.38×10^{-23} J K^{-1}, T is temperature 300 K and q is elementary charge quantity 1.602×10^{-19} C. So E_{fb} could be calculated to 0.67 eV.

V_p is the energy difference between the maximum of the p-Si valence band and Fermi level. V_p was obtained from following equation:

$$V_p = \frac{KT}{q} ln(\frac{N_v}{N_q})$$

where N_v is the effective density of states in the p-Si valence band. N_v was obtained from following equation:

$$N_v = \frac{(2m_p^* k_0 T)^{\frac{3}{2}}}{4\pi^{\frac{3}{2}}\hbar^3}$$

In this equation m_p^* is the effective hole mass in the valence band of Si which could be measured as 0.59 m_0. m_0 is the electron mass 9.110×10^{-31} kg. And k_0,π and $\hbar$ are constants. k_0 is Boltzmann constant and $\hbar$ is reduced Planck constant $\frac{h}{2\pi}$. So N_v is related to the temperature which could be calculated to 1.04×10^{19} cm^{-3} at 300 K .

N_q is the dopant concentration of the p-Si which can be mensurated from the slope $\left[\frac{d(\frac{1}{C^2})}{dV}\right]$ -0.9505×10^{16} of the Mott-Schottky plots linear fitting line in Fig. 2a by the following equation:

$$N_q = \frac{2}{e\varepsilon_0\varepsilon}\left[\frac{d(\frac{1}{C^2})}{dV}\right]^{-1}$$

where e is the elementary charge quantity, while the vacuum dielectric constant ε_0 is 8.85×10^{-14} F cm^{-1} and the relative dielectric constant (ε) is 11.68.[1, 2]

The ABPE was calculated from the following equation:

$$ABPE = \frac{|J(mA\ cm^{-2}| \times V_{bias}(V)}{P(mW\ cm^{-2})} \times 100\%$$

where J is the photocurrent density of the photocathode, V_{bias} is the bias potential *vs.* RHE, and P is the power of the illumination (100 mW cm^{-2}).[3]

Measurement of photovoltage

The photovoltage of the photocathode were measured in the same condition as the photoelectrochemical measurements. The photocathode was working electrode while a graphite rod electrode and an SCE electrode were used as the counter electrode and the reference electrode, respectively. The open-circuit potential (V_{ocp}) of the photocathode was measured with different illumination condition. The photovoltage was calculated by the difference between the V_{ocp} with chopped illumination. (Fig. S4)

Measurement of mass activity, EIS, IPCE and Faraday efficiency

According to the fabrication process in the experimental section, a Pt film with thickness of 8 nm was deposited on the p-Si. As the electrochemical activity area was 0.25 cm^2, the volume of deposited Pt could be calculated to be 2×10^{-7} cm^3. The density of Pt is 21.45 g cm^{-3}. Therefore, the mass of deposited Pt could be calculated to be 4.29×10^{-6} g. The control sample Pt NP/$NiSi_2$/p-Si was fabricated according to our previously reported procedure.[4] And the loading amount of Pt in the Pt NP/$NiSi_2$/p-Si was estimated from the SEM image (Fig. S2d of Ref. 4). The particle size ranges from 14.89 to 70.50 nm with an average size of 35.63 nm. As the

deposition area is 0.25 cm^2, the volume loading of Pt particle on $NiSi_2$ is 4.09×10^{-7} cm^3 with the simplification of particles as hemisphere. Therefore, the mass loading of Pt in Pt NP/$NiSi_2$/p-Si is about 8.76×10^{-6} g.

Based on the mass calculated above, the electrocatalytic mass activities of the $Pt_{x(x=2,3)}Si$/PtSi/p-Si and Pt NP/$NiSi_2$/p-Si was investigated according to the formula below (Fig. S8):

$$\text{Mass activity} = \frac{I}{m_{Pt}}$$

which I is current, m_{Pt} is the mass of Pt.

The EIS of the photocathode were measured in the same condition as the photoelectrochemical measurements. The frequency range is 1×10^5 Hz to 25 Hz, and the ac amplitude is 5 mV.

The IPCE of the photocathode were measured at a bias of -0.256 V *vs.* RHE in 0.5 M H_2SO_4 under the illumination in a range of 450 nm and 1000 nm. Under the illumination of a 500 W xenon lamp, the light of different wavelengths was generated through a monochromator (Beijing Hongyuan WDG30). The IPCE was calculated by the following formula, which is shown in Fig. S10a:

$$\text{IPCE} = \frac{1240 \times J}{\lambda \times P_{light}}$$

which J is electric current; λ is incident light wavelength and P_{light} is the power of incident light.

The mixed gas generated during the chronoamperometry test was collected by the drainage method. And the Faraday efficiency was calculated by the following formula:

$$\text{Faraday efficiency} = \frac{m \times n \times F}{I \times t}$$

which m is the mole number of the product, n is the number of reaction electron, F is Faraday constant 96485 C mol^{-1}, I is electric current and t is reaction time.

The m could be calculated by the collection volume of mixed gas, and I×t could be calculated by the integration of chronoamperometry curve.

Supplementary Figures

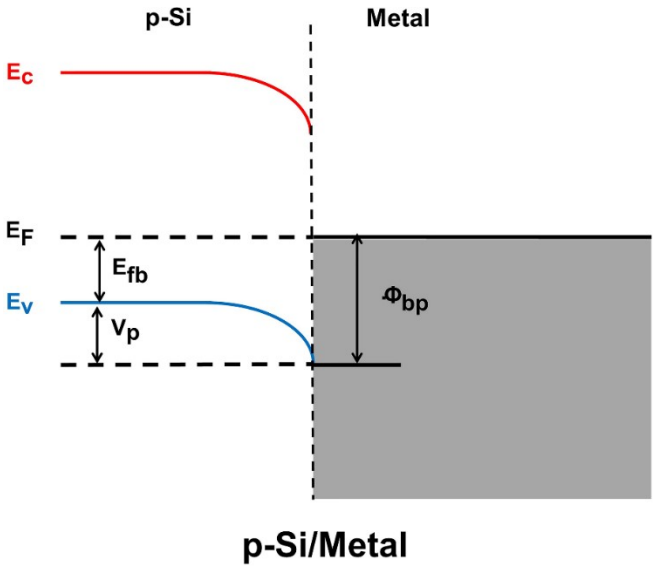

Fig. S1 Schematic illustration of energy band structure of a metal/p-Si Schottky junction.

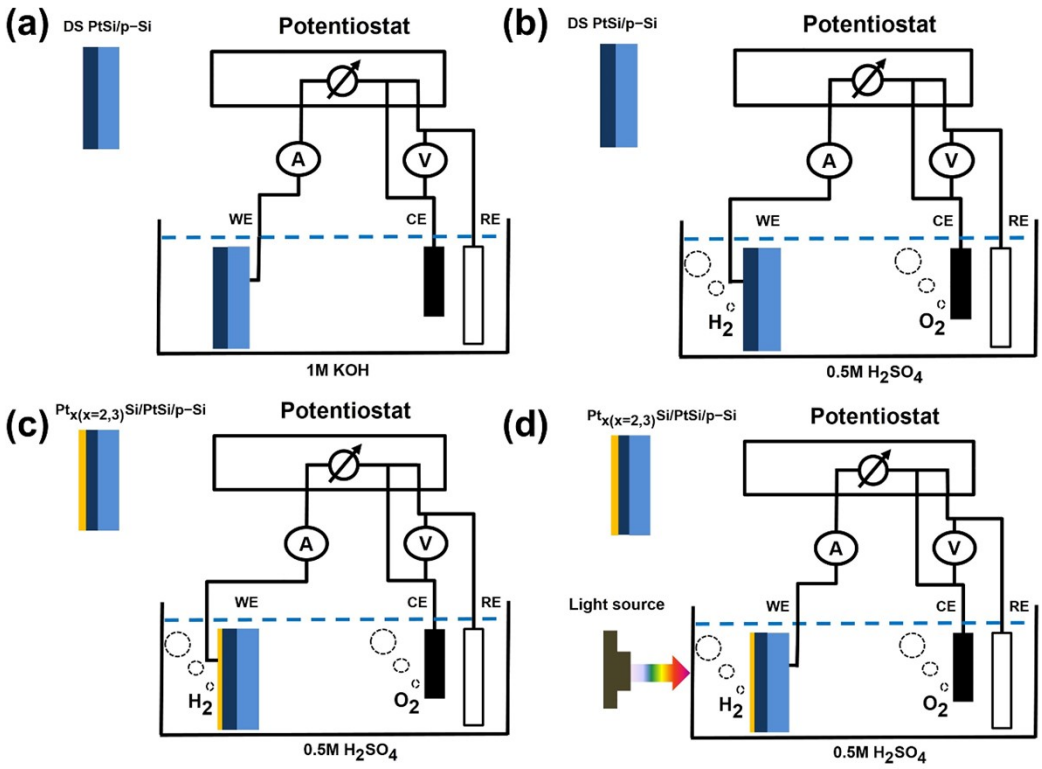

Fig. S2 Schematic illustration of electrochemical surface reconstruction (ESR), electrochemical (EC) measurement and photoelectrochemical (PEC) measurement. (a) Schematic illustration of ESR on DS PtSi/p-Si; (b) Schematic illustration of EC measurement of the PtSi;(c) Schematic illustration of EC measurement of the $Pt_{x(x=2,3)}Si$; (d) Schematic illustration of PEC measurement of $Pt_{x(x=2,3)}Si/PtSi/p-Si$.

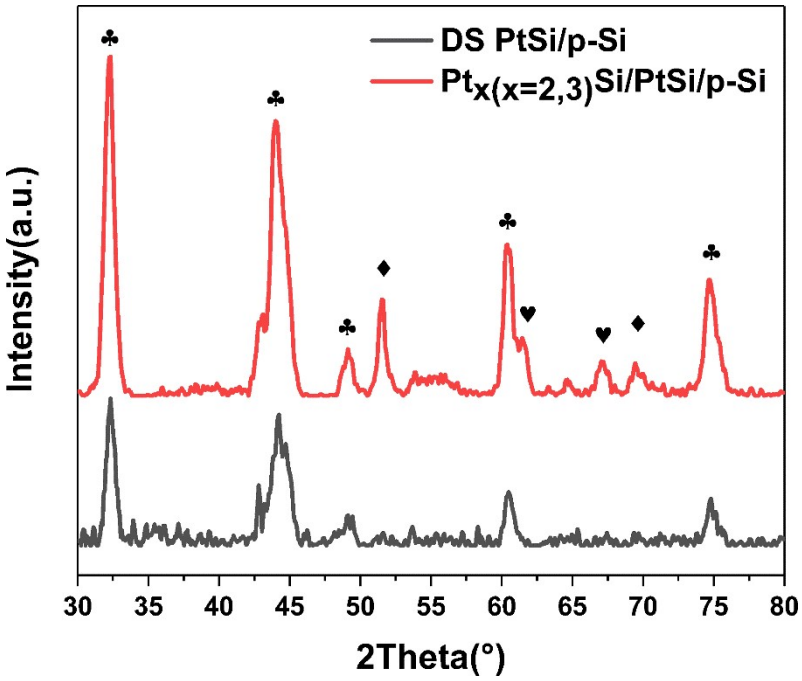

Fig. S3 GI-XRD patterns of DS PtSi/p-Si (black) and $Pt_{x(x=2,3)}Si$/PtSi/p-Si (red), the characteristic peaks of PtSi (♣ JCPDS#07-0251) Pt_2Si (♥ JCPDS#17-0683) and Pt_3Si (♦ JCPDS#34-0956) were shown.

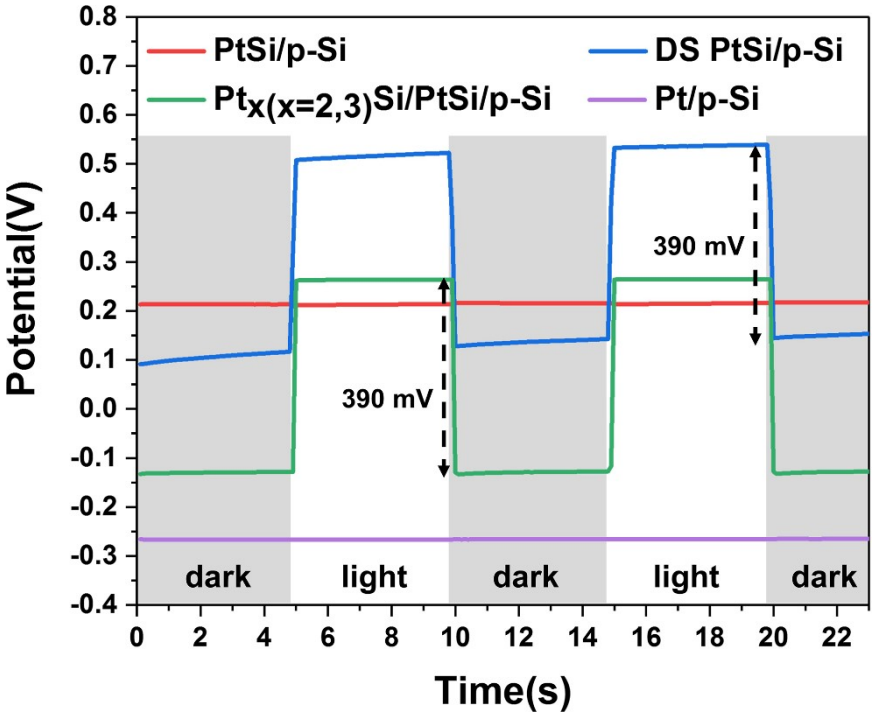

Fig. S4 The V_{ocp}-t curves of PtSi/p-Si (red), DS PtSi/p-Si (blue), $Pt_{x(x=2,3)}Si$/PtSi/p-Si (green) and Pt/p-Si (purple) in 0.5 M H_2SO_4 recorded under chopped illumination.

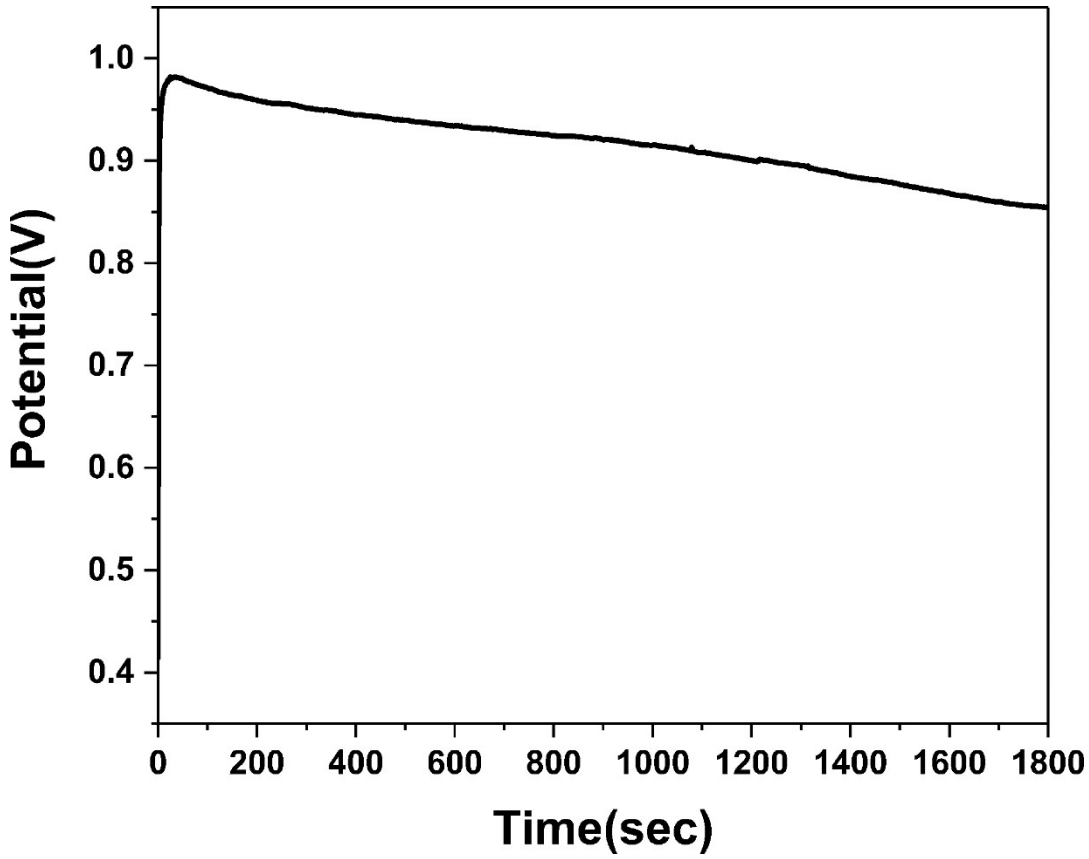

Fig. S5 Chronopotentiometry of electrochemical surface reconstruction (ESR) at 0.01 mA for 30 minutes in 1 M KOH solution.

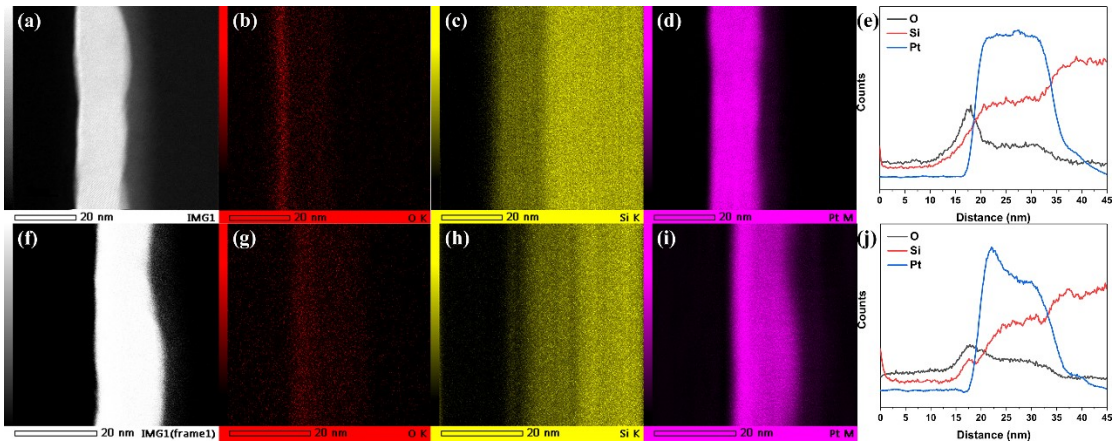

Fig. S6 STEM images, EDS mapping images and EDS line scan curves of DS PtSi/p-Si (a-e) and $Pt_{x(x=2,3)}Si$ /PtSi/p-Si (f-j). (a): STEM image; (b) O, (c) Si, (d) Pt; (e) EDS line scan curves; (f) STEM image; (g) O, (h) Si, (i) Pt; (j) EDS line scan curves.

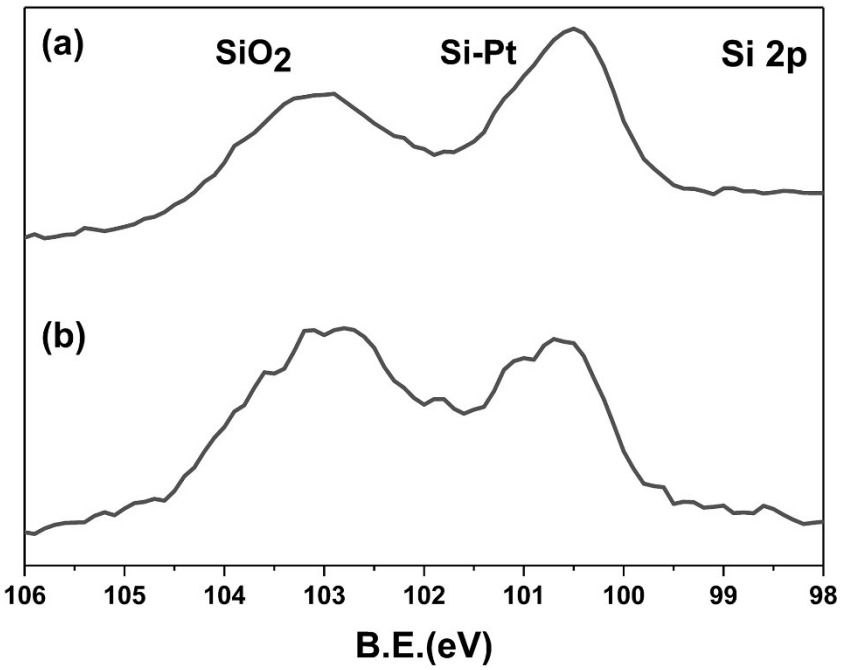

Fig. S7 Si 2p XPS spectra recorded from the photoelectrode before and after ESR. (a) DS PtSi/p-Si photocathode, (b) $Pt_{x(x=2,3)}Si$ /PtSi/p-Si photocathode.

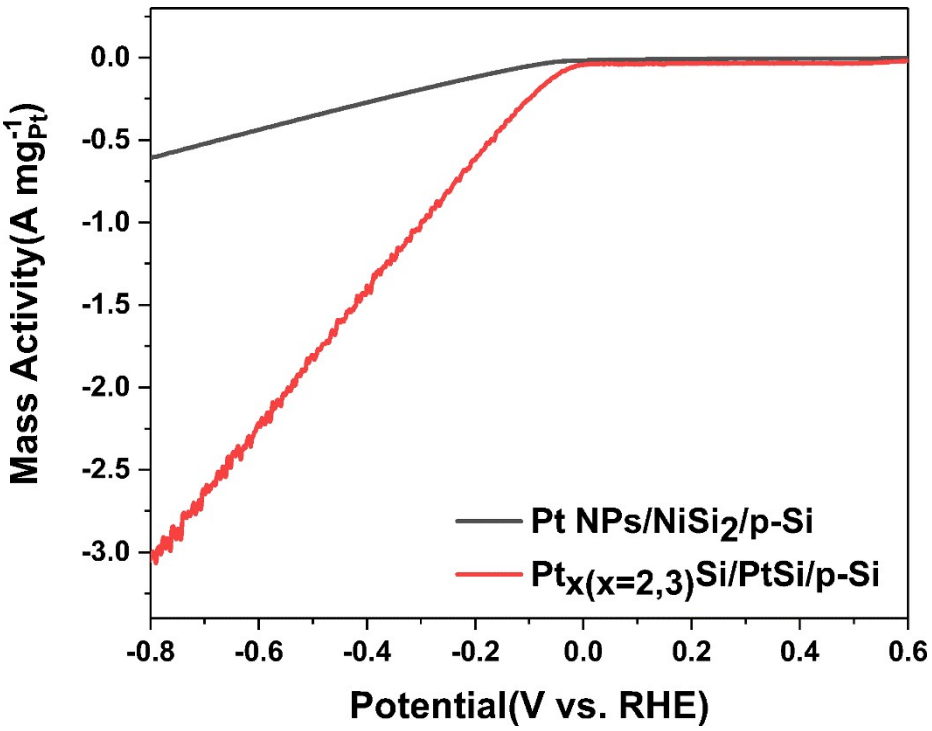

Fig.S8 Mass electrochemical activity of the $Pt_{x(x=2,3)}Si$/PtSi electrode (red) and Pt NPs/$NiSi_2$ electrode (black) in 0.5 M H_2SO_4 electrolyte.

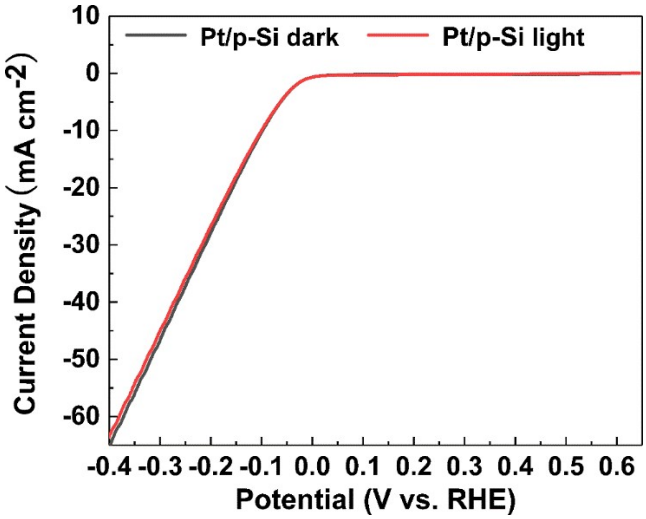

Fig. S9 LSV curves of the Pt/p-Si measured in 0.5 M H_2SO_4 solution in dark and under AM 1.5 illumination with intensity of 100 mW cm^{-2}.

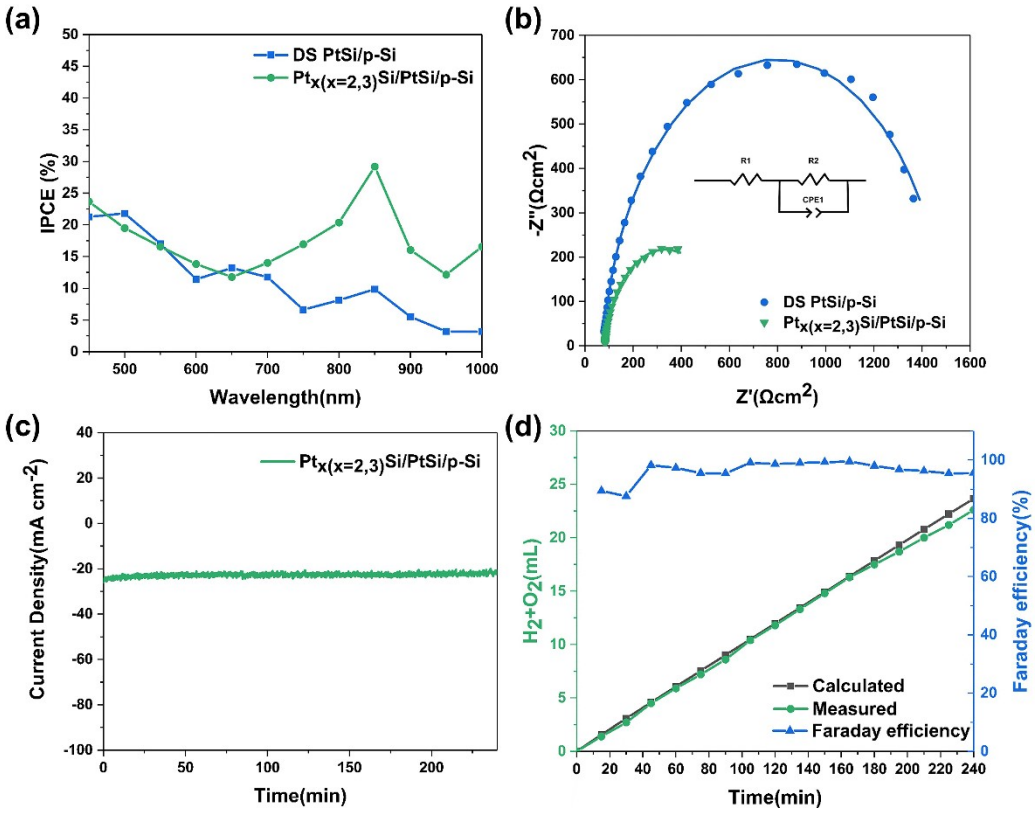

Fig. S10 (a) IPCE spectra of DS PtSi/p-Si and $Pt_{x(x=2,3)}Si/PtSi/p-Si$ in 0.5 M H_2SO_4 at -0.256 V *vs.* RHE; (b) EIS spectra of DS PtSi/p-Si (blue) at -0.056 V *vs.* RHE and $Pt_{x(x=2,3)}Si/PtSi/p-Si$ (green) at 0.444V *vs.* RHE in 0.5 M H_2SO_4 under illumination. The dots are experimental data and the solid lines are simulation curves based on the equivalent circuit showing in the inset of the figure; (c) Chronoamperometry measurements of the $Pt_{x(x=2,3)}Si/PtSi/p-Si$ at -0.056 V *vs.* RHE in 0.5 M H_2SO_4 solution under illumination; (d) The measured and theoretical volume of the mixed gas of hydrogen and oxygen generated during the chronoamperometry test and Faraday efficiency.

Supplementary Table

Summary various representative Si-based photocathodes without p-n junction applying Pt catalyst (NP:nanoparticles; NW:nanowires; NR:nanorods)

Structure	Onset potential (V *vs.* RHE)	Current densities at 0 V *vs.* RHE (mA cm^{-2})	Saturated photocurrent (mA cm^{-2})	ABPE (%)	References
Pt NP/p-Si	0.3	-10	-10		[5]
Pt NP/p-Si	0.24	-2	-2		[6]
Pt NP/p-Si NW	0.4	-17	-17		[7]
Pt NP/TiO_2 NW/p-Si	0.25	-20.7	-30		[8]
Pt NP/SiO_x NW/p-Si	0.35	-9.1	-10		[9]
Pt/p-Si NW	0.48	-12.8	-14.3	1.2	[10]
Pt/Ti/SiO_2/p-Si	0.5	-18	-20	2.9	[11]
Pt/TiO_2 NR/p-Si	0.44	-40	-40	2.5	[12]
Pt/Al_2O_3/p-Si	0	0	-27		[13]
Pt/Ti/$SrTiO_3$/p-Si	0.45	-15	-35	4.9	[14]
TiO_2/Pt NP/p-Si	0.37	-7.5	-27		[15]
SiO_x/Pt/p-Si	0.2	-30	-33		[16]
Pt/Graphene/p-Si	0.4	-32	-32		[17]
Ag-Pt/SiO_x/p-Si	0.36	-30	-35		[18]
Pt NP/$NiSi_2$/p-Si	0.53	-36	-37	5.2	[19]
$Pt_{x(x=2,3)}Si$/PtSi/p-Si	0.54	-30	-30	5.8	This work

References

1. S. Li, G. She, C. Chen, S. Zhang, L. Mu, X. Guo and W. Shi, *ACS Appl. Mater. Interfaces*, 2018, **10**, 8594-8598.
2. J. Luo, Z. Qiu, J. Deng, C. Zhao, J. Li, W. Wang, D. Chen, D. Wu, M. Östling, T. Ye and S. Zhang, *Microelectron Eng*, 2014, **120**, 174-177.
3. R. Fan, Z. Mi and M. Shen, *Opt. Express*, 2019, **27**, A51-A80.
4. S. Li, H. Zhang, G. She, J. Xu, S. Zhang, Y. Deng, L. Mu, Q. Zhou, Y. Liu, J. Luo and W. Shi, *ACS Applied Energy Materials*, 2021, **4**, 11574-11579.
5. C. U. Maier, M. Specht and G. Bilger, *Int. J. Hydrogen Energy*, 1996, **21**, 859-864.
6. I. Lombardi, S. Marchionna, G. Zangari and S. Pizzini, *Langmuir*, 2007, **23**, 12413-12420.
7. I. Oh, J. Kye and S. Hwang, *Nano Lett.*, 2012, **12**, 298-302.

8. N. P. Dasgupta, C. Liu, S. Andrews, F. B. Prinz and P. Yang, *J. Am. Chem. Soc.*, 2013, **135**, 12932-12935.
9. P. Dai, J. Xie, M. T. Mayer, X. Yang, J. Zhan and D. Wang, *Angew. Chem., Int. Ed. Engl.*, 2013, **52**, 11119-11123.
10. U. Sim, H.-Y. Jeong, T.-Y. Yang and K. T. Nam, *J Mater Chem A*, 2013, **1**, 5414-5422.
11. D. V. Esposito, I. Levin, T. P. Moffat and A. A. Talin, *Nat. Mater.*, 2013, **12**, 562-568.
12. D. M. Andoshe, S. Choi, Y.-S. Shim, S. H. Lee, Y. Kim, C. W. Moon, D. H. Kim, S. Y. Lee, T. Kim, H. K. Park, M. G. Lee, J.-M. Jeon, K. T. Nam, M. Kim, J. K. Kim, J. Oh and H. W. Jang, *J Mater Chem A*, 2016, **4**, 9477-9485.
13. M. J. Choi, J. Y. Jung, M. J. Park, J. W. Song, J. H. Lee and J. H. Bang, *J Mater Chem A*, 2014, **2**, 2928–2933.
14. L. Ji, M. D. McDaniel, S. Wang, A. B. Posadas, X. Li, H. Huang, J. C. Lee, A. A. Demkov, A. J. Bard, J. G. Ekerdt and E. T. Yu, *Nat. Nanotechnol.*, 2015, **10**, 84-90.
15. S. Li, P. Zhang, X. Song and L. Gao, *ACS Appl. Mater. Interfaces*, 2015, **7**, 18560-18565.
16. N. Y. Labrador, X. Li, Y. Liu, H. Tan, R. Wang, J. T. Koberstein, T. P. Moffat and D. V. Esposito, *Nano Lett.*, 2016, **16**, 6452-6459.
17. C. K. Ku, P. H. Wu, C. C. Chung, C. C. Chen, K. J. Tsai, H. M. Chen, Y. C. Chang, C. H. Chuang, C. Y. Wei, C. Y. Wen, T. Y. Lin, H. L. Chen, Y. S. Wang, Z. Y. Lee, J. R. Chang, C. W. Luo, D. Y. Wang, B. J. Hwang and C. W. Chen, *Adv. Energy Mater.*, 2019, **9**, 1901022-1901031.
18. S. Y. Lim, K. Ha, H. Ha, S. Y. Lee, M. S. Jang, M. Choi and T. D. Chung, *Phys. Chem. Chem. Phys.*, 2019, **21**, 4184-4192.
19. S. Li, H. Zhang, G. She, J. Xu, S. Zhang, Y. Deng, L. Mu, Q. Zhou, Y. Liu, J. Luo and W. Shi, *ACS Applied Energy Materials*, 2021, DOI: 10.1021/acsaem.1c02318.